Phys Chem Minerals (2001) 28: 188–198

ORIGINAL PAPER

D. E. Harlov · M. Andrut · B. Pöter

Characterisation of buddingtonite $(NH_4)[AlSi_3O_8]$ and ND_4-buddingtonite $(ND_4)[AlSi_3O_8]$ using IR spectroscopy and Rietveld refinement of XRD spectra

Received: 5 October 1999 / Accepted: 1 November 2000

Abstract Buddingtonite $(NH_4)[AlSi_3O_8]$ and its deuterated analogue ND_4-buddingtonite $(ND_4)[AlSi_3O_8]$ have been synthesised in 150-mg amounts at 500 and 400 °C and 500 MPa in 5-mm-wide, 4-cm-long Au capsules using René metal hydrothermal autoclaves. The resultant product consists of clumps of monoclinic crystals with diameters of 30–60 μm. The ND_4-buddingtonite contains minor amounts of NH_4-buddingtonite due to H_2 migration across the Au membrane. Using this synthesis technique resulted in $>99\%$ pure buddingtonite in 20% of the synthesis runs with the remaining synthesis runs containing very minor tobelite and quartz on the order of a few percent. IR spectra obtained from powdered samples are assigned on the basis of T_d symmetry for the ammonium molecule. They show triply degenerate vibrational bands (i.e. ν_3 and ν_4) and some overtones and combination modes from NH_4^+ and ND_4^+. While T_d symmetry for NH_4^+ in buddingtonite is not completely correct due to distortion of the NH_4^+ molecule, the non-cubic field is not large enough to cause a substantial splitting in the bands. However, this perturbation is documented in the IR spectra by a substantial increase in the FWHH as well as the occurrence of shoulders on the broadened bands. Rietveld analysis indicates that buddingtonite, like orthoclase, has a monoclinic structure with space group symmetry $C2/m$. Here, the NH_4^+ molecule replaces the K^+ cation on the nine fold coordinated A site which has m symmetry. Due to the larger size of the NH_4^+ molecule, the N–O interatomic distances are larger than the K–O distances in pure orthoclase and range from 2.95 to 3.16 Å. This results in an increase in the volume of the polyhedron hosting the NH_4^+ molecule. Also, in contrast to orthoclase, the polyhedron hosting the NH_4^+ molecule becomes more regular. The rigid Al, Si tetrahedra of the framework adjust to this expansion of the A site by rotation. This results in larger unit cell parameters for buddingtonite when compared to natural and synthesised potassium feldspars. This increase is especially seen with respect to the lattice constants a and b and the monoclinic angle β which also are found to be extremely variable. In contrast, the c direction remains nearly unchanged. Investigations using IR spectroscopy indicate that it is unlikely that this variation in the a, b and β cell dimensions is caused by incorporation of H_3O^+ or zeolitic water. Instead, it is more likely that substitution of NH_4^+ for K^+ coupled with Al, Si disorder are the chief contributors to these variations in the unit cell parameters for buddingtonite.

Key words Buddingtonite · ND_4-buddingtonite · Feldspar · Ammonia · IR spectroscopy · Rietveld analysis

D. E. Harlov (✉) · B. Pöter
GeoForschungsZentrum Potsdam, Telegrafenberg, 14473 Potsdam, Germany
e-mail: dharlov@gfz-polsdam.de
Fax: +49 288 1402

M. Andrut
Institute for Mineralogy and Crystallography, University of Vienna – Geozentrum, 1090 Vienna, Austria

Introduction

In nature, buddingtonite, $(NH_4)[AlSi_3O_8]$, is the ammonium analogue of K-feldspar. Due to their relatively similar sizes, the NH_4^+ molecule (1.69 Å for a ninefold coordination) can substitute for the K^+ cation (1.52 Å) on the A site in the orthoclase structure. Ammonium analogues in the silicate minerals are also seen in the feldspathoids with the occurrence of ammonioleucite $(NH_4)[AlSi_2O_6]$ (Hori et al. 1986) and in muscovite with the occurrence of tobelite $(NH_4)[Al_3Si_3O_{10}]$ $(OH)_2$ (Higashi 1982).

Near-surface formation of buddingtonite or NH_4^+ enrichment in K-feldspar can be the result of ion exchange between K-feldspar and/or possibly plagioclase and ammonium-rich fluids under highly reducing conditions, generally at temperatures below 100 °C. For example, natural occurrences of buddingtonite were first described by Erd et al. (1964) and Barker (1964) in samples of andesitic rocks taken from ammonia-rich hot springs. Here, it was described as a pseudomorphus replacement after plagioclase in hydrothermally altered andesitic rocks below the water table. Subsequently, buddingtonite was found associated with other ammonium-rich hot springs (Krohn and Altaner 1987; Krohn et al. 1993). In addition, hydrothermal alteration of granitic rocks due to ammonium-enriched circulating groundwaters in contact with organic-rich source rocks, such as black shales or coal deposits, can subsequently enrich the K-feldspar in NH_4^+ (Hall 1993).

Buddingtonite can also form in association with diagenetic processes in highly reducing ammonia-rich environments, again under relatively low temperatures (<300 °C) and pressures (<200 MPa), as an apparent natural growth of feldspar. In general, the highly reducing nature of these environments is governed by the presence of black shales and/or coal deposits in direct contact either with or via circulating groundwaters. For example, in arkosic sandstones of the San Joaquin and Los Angeles Basins, buddingtonite occurs as an early diagenetic phase in the form of microfracture fillings and overgrowth on detrital K-feldspar as a result of hydrothermal exchange with organic-rich highly reduced shales (Ramseyer et al. 1993). Buddingtonite has also been found in solid solution with K-feldspar in mudstones from the Phosphoria Formation located in southeastern Idaho (Gulbrandsen 1974), again under highly reducing conditions. In oil shale deposits from Queensland, Australia, buddingtonite averages 10% of the strata and most likely had its origins in ammonia-rich reduced muds beneath a stratified lake (Loughnan et al. 1983). In Tertiary pyroclastic rocks from Greece which have undergone diagenesis, newly formed K-feldspar shows definite enrichment in NH_4^+ (Hall et al. 1994). This diagenetic alteration is also seen in Middle Triassic tuffaceous rocks located in central Spain (Marfil et al. 1998). Here, the authigenic K-feldspars in the underlying arkosic sandstones have a NH_4^+ content ranging from 48 to 191 ppm.

In non-reduced metamorphic and igneous rocks within ± 1 $\log_{10}$ unit of the Ni–NiO oxygen buffer, K-feldspar can contain traces of NH_4^+ up to several 100 ppm (Honma and Itihara 1981). After biotite-phlogopite and muscovite, it is the largest source of nitrogen in both high-grade metamorphic rocks and igneous rocks such as granites and pegmatites (Honma and Itihara 1981; Solomon and Rossman 1988; Hall 1988a, b; Hall et al. 1996). As a consequence, NH_4^+ in K-feldspar could serve as an important reservoir of nitrogen in the lower crust.

Like orthoclase, buddingtonite is monoclinic with a $C2/m$ space group symmetry (Kimball and Megaw 1974; Voncken et al. 1988, 1993). While buddingtonite was initially believed to contain zeolitic H_2O (Barker 1964), this has since been shown to be incorrect by Voncken et al. (1993) in an IR spectroscopic and thermal gravimetric study. However, a recent study by Laricheva et al. (1993, 1996) suggests that buddingtonite synthesised under relatively low temperatures (250–450 °C) and pressures (100 MPa) from gels can contain some zeolitic H_2O. Because of the relatively small size of the synthesised individual crystals (<50 μm), most IR investigations have been performed on powders only. Both Erd et al. (1964) and Voncken et al. (1993) have recorded individual IR absorption band positions for buddingtonite; however, they only noted whether these were due to either stretching or bending of the N–H bonds. With respect to the study of Erd et al. (1964), these absorption bands were partially obscured by O–H-stretching vibrational bands due to the presence of zeolitic water. So far, the one single-crystal IR study of a feldspar phase containing NH_4^+ has been on a natural hyalophane feldspar from Zagrlski Potok, Bosnia (Beran et al. 1992).

Buddingtonite was previously synthesised by Hallam and Eugster (1976), Voncken et al. (1988, 1993) and Laricheva et al. (1993, 1996) from either gels or oxide mixes in an NH_3- rich environment generally buffered to highly reducing conditions using graphite/CH_4-buffered setups. Buddingtonite can also be synthesised by exchange between natural sanidine or orthoclase and an NH_3-rich solution or NH_4Cl, again buffered to highly reducing conditions (Barker 1964). Synthesis conditions generally range from 250–660 °C and 50–200 MPa. Whereas infra red (IR) spectra of ammonium in both synthetic and natural buddingtonite have been described by Voncken et al. (1988, 1993), none of the observed bands has been assigned transitions. In addition, powder X-ray diffraction spectra (XRD) of buddingtonite, whether synthetic or natural, have never been refined using the Rietveld technique. ND_4-buddingtonite has never been characterised using IR spectroscopy and/or powder XRD spectra analysis including the Rietveld refinement.

In this study we have synthesised both buddingtonite and ND_4-buddingtonite for purposes of characterisation of their crystal chemistry using both IR spectroscopy down to 77 K as well as Rietveld refinement of powder XRD spectra. A second aim of this study is to serve as a basis for future investigations of the ND_4 molecule in the buddingtonite structure using more sophisticated techniques, such as neutron diffraction and NMR at temperatures below 77 K. Lastly, the buddingtonite described here is currently being used in a series of experiments charting out the phase equilibria between buddingtonite, tobelite $(NH_4)Al_2[AlSi_3O_{10}](OH)_2$, quartz and Al_2SiO_5.

Experimental procedure

Synthesis

Buddingtonite was synthesised in 150-mg amounts using a stoichiometric Al_2O_3–SiO_2 mix and a 25% NH_3 solution in excess such that the amount of NH_4^+ stoichiometrically available was 50% greater than that needed for the actual synthesis. The Al_2O_3–SiO_2 mix (weighed out to ± 0.05 mg) consisted of grinding the α-Al_2O_3

and SiO_2 together in 1-g batches in ethanol for 30 min such that they were completely homogenised. Synthesis consisted of placing 150 mg of the dry oxide mix along with 150 mg of 25% NH_3 solution in a 5-mm-wide, 4-cm-long Au tube with a wall thickness of 0.2 mm. The Au tube was then welded shut using an argon plasma torch while immersed in an ice water bath. The sealed Au capsule was placed in a 6-mm-diameter bore, cold seal René metal hydrothermal autoclave with an Ni–NiO filler rod and an external NiCr thermocouple. The synthesis run was then taken up initially to 400 or 500 °C and 500 MPa for approximately 1 to 3 weeks. Temperatures were monitored continuously and are believed to be accurate to within ± 3 °C. Pressure was measured using a pressure transducer calibrated against a Heise gauge manometer for which the quoted pressure is accurate to ± 5 MPa. Stability of the growing buddingtonite under the highly reducing conditions needed for its synthesis (Hallam and Eugster 1976) was guaranteed by the internal NH_3-rich fluid which buffered the interior of the capsule via the reaction: $2NH_3 + 3/2O_2 = N_2 + 3H_2O$. However, if left for more than 3 to 4 weeks, the buddingtonite broke down to either tobelite + quartz or to quartz and an Al-silicate mineral, most likely sillimanite-mullite. This is because the interior of the autoclave is effectively buffered to Ni–NiO. The imperfect yet persistent H_2 transfer properties of the Au membrane meant that if left long enough, the NH_3 in solution in the interior of the capsule was completely oxidised to $N_2 + H_2O$ and, consequently, the solution was no longer reducing enough for the buddingtonite to be stable. The synthesis run was quenched using air cooling. This ensured that the interior of the autoclave cooled down to 100 °C within 2–3 min of initial quench. In a successful synthesis run, the resultant charge consisted of > 99% pure buddingtonite in the form of 50 to 100 μm wide clumps of ingrown white monoclinic crystals (cf. Fig. 1a–c). The only impurity in these syntheses was very minor quartz, which was attributed to weighing error. The centre of these clumps was rich in fluid inclusions, indicating rapid nucleation surrounded by very clear inclusion-free thick rims, indicating later slower growth (cf. Fig. 1d). In approximately 80% of the synthesis runs, minor tobelite in abundances ranging from approximately 1 to 10% volunteered along with a corresponding increase in quartz. Minor tobelite also volunteered in synthesis runs at 300–400 °C and 500 MPa. Attempts to discourage the growth of tobelite by saturating the solution with SiO_2 for synthesis runs at 300, 400 and 500 °C and 500 MPa still resulted in tobelite volunteering – again in minor amounts (1–5%). This would suggest that at these temperatures and pressures, buddingtonite may actually be a metastable phase with respect to tobelite + quartz. Attempted

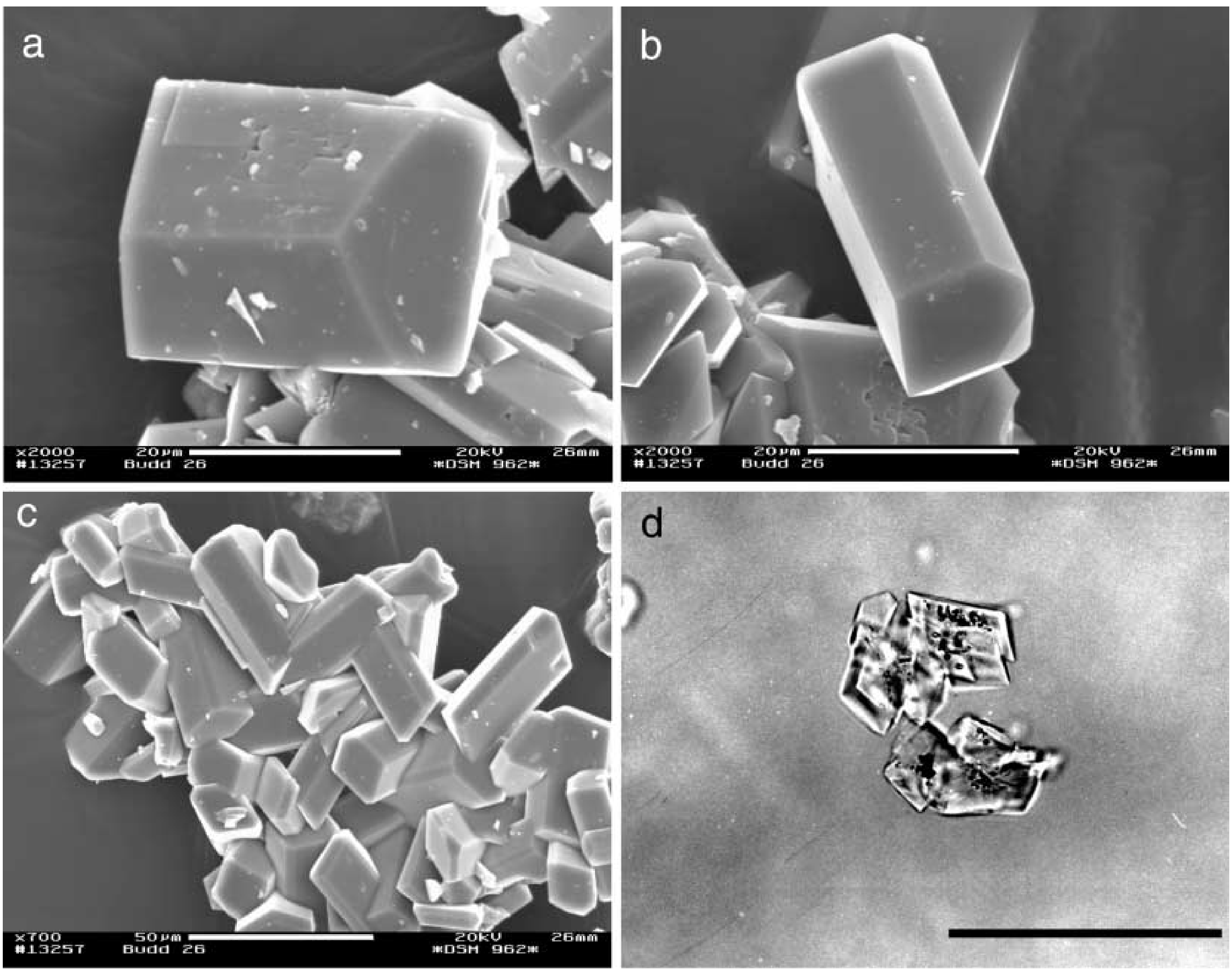

Fig. 1 **a, b** SEM photographs of individual buddingtonite crystals showing monoclinic symmetry at different orientations with respect to the c axis. **c** SEM photograph of a typical clump of intergrown buddingtonite crystals which were the most common form of buddingtonite for synthesis runs at 500 and 400 °C. **d** Transmitted light photograph of buddingtonite crystal clumps in refractive index oil ($n = 1.518$). Note the numerous fluid inclusions in the cores of the buddingtonite crystals which are subsequently surrounded by thick clear rims. *Bar* 50 μm

synthesis of buddingtonite at 600 °C and 500 MPa always resulted in a large tobelite fraction volunteering (20–30%) along with co-existing buddingtonite and quartz. Lastly, using a standard salt setup and a 22-mm-diameter non-endloaded, two-piston piston-cylinder apparatus (Johannes 1973), a 3-mm-diameter Au capsule with starting materials consisting of AlN, SiO_2 and H_2O was arc-welded shut and taken up to 600 °C and 1000 MPa for 4 days. Products from this synthesis run consisted of buddingtonite, tobelite and quartz.

Synthesis of ND_4-buddingtonite was carried out in much the same way, here at 500 °C and 500 MPa. The principal difference was the use of a 26% solution of ammonium deuteride, i.e. ND_3, in D_2O. Other differences included using a new dry syringe for loading the 26% ND_3 solution into the Au capsule previously dried at 105 °C overnight, and synthesis runs of only 1 week. This was done to ensure minimal migration of H_2 cations across the Au membrane into the Au capsule and minimal migration of D_2 out, thus limiting contamination of the ND_4-buddingtonite with H_2 as much as possible. One week was necessary to ensure complete crystallisation of the ND_4-buddingtonite. Even so, IR spectroscopy indicated a definite NH_4-buddingtonite component in each of the three ND_4-buddingtonite synthesis runs attempted.

IR spectroscopy

The nature and size of the synthesised crystal clumps for either the NH_4- or ND_4-buddingtonite were too small to allow for single-crystal measurements (cf. Fig. 1). As a consequence, only powdered samples could be investigated. Samples for IR absorption measurements were prepared by grinding 5 mg (>99% pure) NH_4- or ND_4-buddingtonite and dispersing it into 450 mg of KBr. The homogenised mixture was then pressed into 13-mm-diameter transparent pellets under vacuum and then dried for several days at 170 °C. No recognisable difference was seen between the IR spectrum of a powdered sample taken using an IR microscope as compared to a sample dispersed in a prepared KBr pellet. This indicates that no measurable exchange between the K in the KBr and the NH_4^+ or ND_4^+ in the buddingtonite took place. The KBr pellet technique was used since it provides the best way to disperse and dilute the sample.

Absorption measurements were carried out in the spectral range 3800 cm^{-1} to 800 cm^{-1} with a resolution of 1 cm^{-1} using a Bruker IFS 66v FTIR spectrometer equipped with a globar as the light source, a KBr beam-splitter and DTGS detector. Spectra were averaged over 256 scans. Phase correction mode of the interferogram was performed using the procedure after Mertz (1965) (Griffiths and de Haseth 1986). Norton-Beer weak mode was chosen as the apodisation function. The sample chamber of the Bruker IFS 66v was evacuated down to 200 Pa. Therefore, the influence of H_2O vapour and CO_2 is negligible. In order to study their behaviour at low temperature, samples were cooled to 77 K within the evacuated sample chamber of the FTIR spectrometer using liquid N_2 in an internal cooling device. The spectra are displayed in the form of absorption spectra versus wave number. After background correction, the band centre, full width at half height (FWHH) and integral intensity of each absorption band were determined using the program PeakFit by Jandel Scientific. IR spectra for both the buddingtonite and ND_4-buddingtonite are given in Table 1 and in Figs. 2–4.

X-ray analysis

Determination of phases present in the charge was accomplished using powder X-ray diffraction analysis. For this purpose 1 or 2 mg of the charge were ground in an agate mortar to a grain size of less than 2 µm. The powder was diluted with Elmer's White Glue and mounted on a circular foil. Powder XRD patterns were recorded in transmission using a fully automated STOE STADI P diffractometer (Cu $K_{\alpha 1}$ radiation) equipped with a primary monochromator and a 7°-position sensitive detector (PSD). Operating conditions were 40 kV and 40 mA with a takeoff angle of 6°. The spectra were

Table 1 Band assignments for vibrational modes (ν) with respect to centres, FWHH (FW) in cm^{-1} and relative intensities (Int). *sh* – shoulder; *w* – weak; *m* – medium; *s* – strong; *x* – not observed

ν (cm^{-1})	$(NH_4)^+$	NH_4Cl (298 K)			Buddingtonite B3 (298 K)			Buddingtonite Menlo Park, California (298 K)			ND_4-Buddingtonite N–H vib. (298 K)			ND_4-Buddingtonite N–D vib. (298 K)			ND_4-Buddingtonite N–D vib. (77 K)		
	Centre	Centre	FW	Int	Centre	FW	Int	Centre	FW	Int	Centre	FW	Int	Centre	FW	Int	Centre	FW	Int
ν_4	1400	1400	25	s	1440	60	m	1435	45	s	1430	50	w	1080	50	w	x		
		x			1480 sh		w	1475 sh		w	x			x			x		
ν_2	1680[a]	x			x			x			x			x			x		
$2\nu_4$		2810	100	w	2845	130	m	2863	115	m	2830	70	w	2155	65	w	2190	50	w
$\nu_2 + \nu_4$		3015	130	m	3045	220	m	3072	185	m	3080	115	w	2265	115	w	2280	90	w
$2\nu_2$		x			3180 sh		w	3190 sh		w	3180 sh		w	2365 sh		m	2360 sh		m
ν_3	3145	3140	130	s	3295	240	s	3295	150	s	3290	115	w	2465	135	s	2470	120	s
		x						3440 sh	x	w				2690 sh			x		
		x						3620 sh		w				2825 sh		w	x		

[a] Raman-active

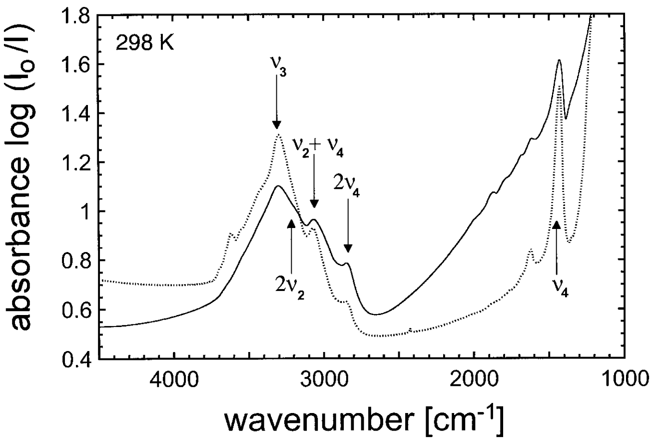

Fig. 2 Normal modes, on the basis of T_d symmetry, are given for IR spectra of natural buddingtonite from Menlo Park, California (*dotted line*), and synthetic buddingtonite (B3) (*solid line*) at 298 K. See text for a description of the various band assignments

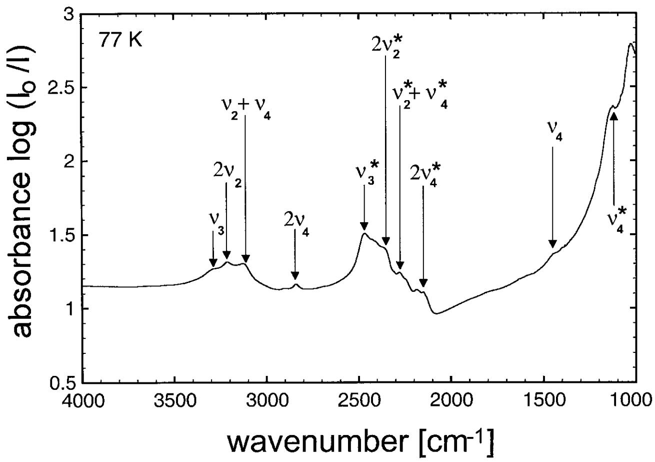

Fig. 4 Normal modes, on the basis of T_d symmetry, are given for an IR spectrum of synthetic ND_4-buddingtonite at 77 K. Absorption bands due to N–D vibrations are marked with an *asterix*. See text for a description of the various band assignments

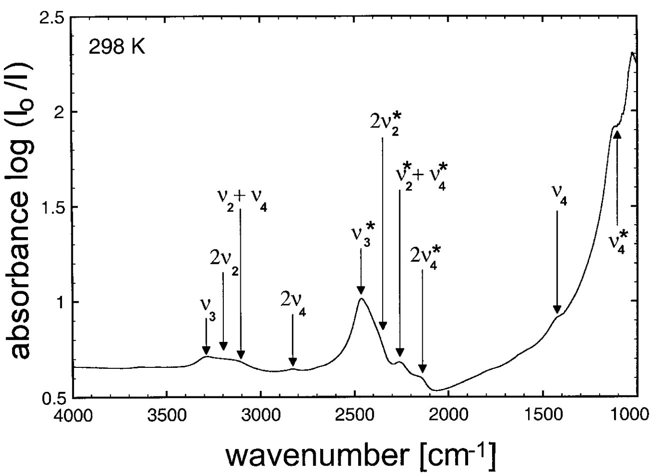

Fig. 3 Normal modes, on the basis of T_d symmetry, are given for an IR spectrum of synthetic ND_4-buddingtonite at 298 K. Absorption bands due to N–D vibrations are marked with an *asterix*. See text for a description of the various band assignments

recorded in the range of 5 to 125° (2θ) using a step interval of 0.1°. The resolution of the PSD was set to 0.02°. Counting times were selected to yield a maximum intensity of 2000 to 3000 counts for each sample, resulting in 5 to 20 s per detector step.

Unit-cell dimensions, additional structural parameters and quantitative phase analysis were determined using the Rietveld analysis technique contained in the GSAS software package (Larson and Von Dreele 1987). For starting values we chose unit-cell parameters, atomic coordinates and isotropic displacement factors for the monoclinic structure ($C2/m$) of orthoclase as given by Chao et al. (1940). The number of profile parameters used was 21 to 23. These consisted of 16 to 18 parameters to fit the background using a real space correlation and five parameters to define the peak form as a pseudo-Voigt with a variable Lorentzian character. No parameters describing peak asymmetry were necessary, because the peak shape is highly symmetric due to the geometry of the STOE STADI P diffractometer. The preferred orientation was corrected using the formulation of March (1932) and Dollase (1986). During the refinement of the XRD spectra, scale factor, background, zero-point correction, unit-cell parameters, phase proportions, preferred orientations, profile parameters and atomic positions were all taken into account. The atom fractions and isotropic displacement factors were not refined. For the refinement we assumed an ideal orthoclase stoichiometry. The XRD spectra and corresponding Rietveld refinement for representative buddingtonite and ND_4-buddingtonite syntheses runs are shown in Fig. 5 and summarised in Tables 2–4.

Electron microprobe analysis

Electron microprobe analysis of the synthesised buddingtonite was problematic. While a cross-section of the mounted buddingtonite crystal clumps was certainly large enough, i.e. up to 40–60 μm, (cf. Fig. 1c and 1d), detection of nitrogen using a conventional SX50 Cameca microprobe required specialised measures. These included cooling the stage down to liquid N_2 temperatures via a cold finger and 2-min counting times on a PC1 crystal using 10 keV, 10 nA, 10 μm beam spot. In addition, the carbon coating was kept to a thickness of approximately 10 Å to minimise absorption and scatter of the electron beam. Even so, count rates averaged 30 counts s^{-1}. In addition, the count rate for nitrogen in the buddingtonite decreased during analysis, suggesting that, much like Na in plagioclase, the ammonium in buddingtonite apparently "evaporates" under the bombardment of the electron beam. Despite these problems, multiple microprobe analyses were made for several buddingtonite syntheses (cf. Table 5). Standards included natural microcline for SiO_2 and Al_2O_3 and other synthetic buddingtonites for $(NH_4)_2O$. The stoichiometric analyses for buddingtonite contained in Table 5 strongly supports the conjecture that the buddingtonite contains no appreciable amounts of zeolitic H_2O.

Results and discussion

IR spectroscopy

The free ammonium ion, i.e. the NH_4^+ molecule, has a T_d symmetry giving rise to four normal vibrational modes (Herzberg 1955). These have the representation A_1 (ν_1), E (ν_2), and 2 × T_2 (ν_3 and ν_4). All fundamentals are Raman-active, but only the triply degenerated states are IR-active. The fundamental frequencies for

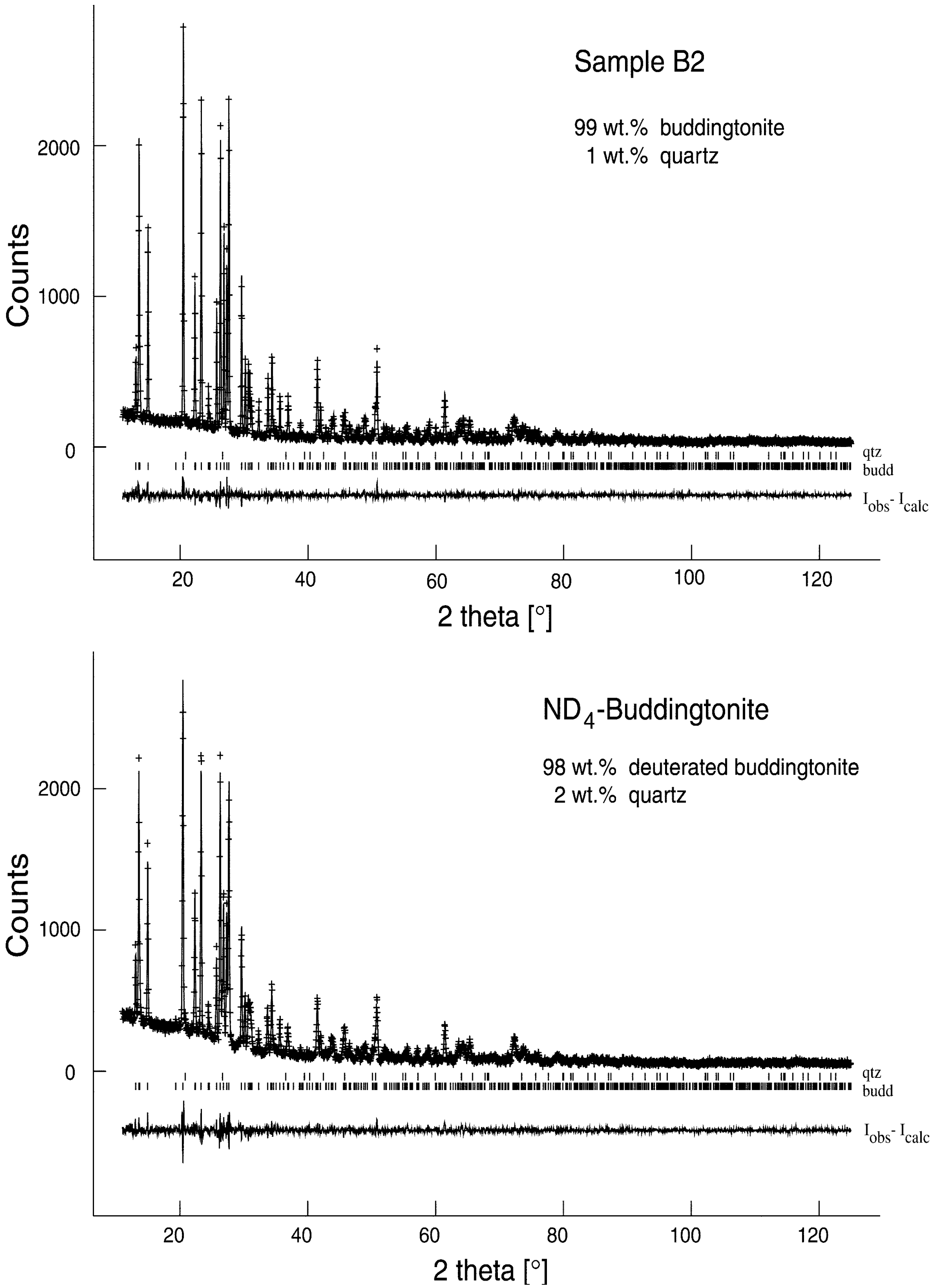

Fig. 5 Rietveld refinement of buddingtonite synthesis B2 and ND_4-buddingtonite showing the accuracy of the refinement

the free ammonium molecule are $\nu_1 = 3040\ \mathrm{cm}^{-1}$, $\nu_2 = 1680\ \mathrm{cm}^{-1}$, $\nu_3 = 3145\ \mathrm{cm}^{-1}$ and $\nu_4 = 1400\ \mathrm{cm}^{-1}$ (Nakamoto 1986 after Landolt-Börnstein 1951). In accordance with selection rules, the IR spectrum of NH_4Cl contains two intense absorption bands which can be assigned to the triply degenerate vibrations ν_3 (stretching) and ν_4 (deformation) of the NH_4^+ molecule (Wagner and Hornig 1950). Additionally, at the low-energy wing of the stretching band ν_3, a combination

Table 2 Rietveld refinement parameters

Phase	R_P	R_{wp}	χ^2	DW	Quantitative phase analysis
Buddingtonite B1	0.062	0.086	1.20	1.63	99 wt% Buddingtonite; 1 wt% Quartz
Buddingtonite B2	0.077	0.106	1.24	1.63	99 wt% Buddingtonite; 1 wt% Quartz
Buddingtonite B3	0.077	0.103	1.36	1.54	84 wt% Buddingtonite; 16 wt% Quartz
Buddingtonite B4	0.051	0.067	1.23	1.55	100 wt% Buddingtonite;
Buddingtonite B5	0.071	0.095	1.33	1.48	99 wt% Buddingtonite; 1 wt% Quartz
Buddingtonite B6	0.062	0.081	1.42	1.38	99 wt% Buddingtonite; 1 wt% Quartz
Deuterated Buddingtonite	0.072	0.093	1.38	1.48	98 wt% Buddingtonite; 2 wt% Quartz
Natural Buddingtonite[a]	0.061	0.079	1.47	1.34	60 wt% Buddingtonite; 35 wt% Quartz; 4 wt% Illite[b]
Orthoclase 1[c]	0.062	0.083	1.19	1.71	100 wt% K-feldspar;
Orthoclase 2[c]	0.067	0.091	1.18	1.68	86 wt% K-feldspar; 14 wt% Quartz

[a] Natural sample from Menlo Park, California
[b] 1 wt% minor phases which could not be identified
[c] Synthesized at 500 °C, 200 MPa from a stoichiometric mixture of SiO_2, Al_2O_3 and K(OH)

mode $\nu_2 + \nu_4$ and the first overtone of the deformation band ν_4 are clearly visible. The behaviour of the NH_4^+ molecule in NH_4Cl at room temperature can be used to describe the N–H vibrational spectrum of both buddingtonite and its deuterated analogue.

Band positions and FWHH for NH_4Cl, both synthetic and natural buddingtonite, and ND_4-buddingtonite are summarised in Table 1. The IR spectra of a natural buddingtonite from Menlo Park, California, and a synthetic buddingtonite (B3) are given in Fig. 2. The IR spectra of ND_4-buddingtonite at 298 and 77 K are displayed in Figs. 3 and 4, respectively. Both natural and synthetic buddingtonite show a broad band at around 1430 cm^{-1} as well as a system of overlapping bands in the spectral region 2700 to 3500 cm^{-1}. These absorption bands are attributed to the presence of NH_4^+. The ND_4-buddingtonite additionally exhibits a system of bands around 2850 to 2200 cm^{-1} and a single absorption band at 1080 cm^{-1} that are due solely to the presence of ND_4^+ (cf. Figs. 3 and 4). The spectrum of ND_4-buddingtonite (Fig. 3) additionally shows weaker absorption bands due to N–H vibrations. This indicates, during synthesis, diffusion of H_2 taking place across the Au membrane into the capsule, as well as possible contamination from atmospheric moisture. While vibrations due to the ND_4^+ molecule are shifted to a lower energy as compared to those for NH_4^+ (cf. Fig. 2 and Table 1), they still show the same basic pattern of absorption bands.

In buddingtonite, the tetrahedral ammonium molecule is situated on the nine-fold co-ordinated A position which has an *m* site symmetry. However, the symmetry of the ammonium molecule on this site is reduced, which causes a further splitting in the former degenerate energy levels (Bastoul et al. 1993). This perturbation of the NH_4^+ tetrahedron is documented in the IR spectra by a substantial increase in the FWHH of the vibrational bands caused by NH_4^+ in comparison to NH_4Cl as well as the occurrence of shoulders on the broadened bands (cf. Table 1 and Fig. 2). This indicates that, while assigning a T_d symmetry to the NH_4^+ molecule is no longer valid (senso stricto), the non-cubic field is not large enough to cause a substantial splitting of the bands. For example, the FWHH of both the ν_3 and ν_4 bands are nearly twice as large as those for NH_4Cl. In addition, they both exhibit shoulders. Further bands, arising from overtones ($2\nu_2$ and $2\nu_4$) and combination modes ($\nu_2 + \nu_4$), are then superimposed on this spectrum (cf. Figs. 2–4). In an IR study of NH_4^+ in a hyalophane feldspar crystal from Zagrlski Potok, Bosnia, Beran et al. (1992) observed a reduction in the T_d symmetry of the NH_4^+ molecule similar to what we have observed here.

Low-temperature IR spectra at liquid N_2 temperatures, i.e. 77 K, for buddingtonite and ND_4-buddingtonite were also obtained. Drying the pellet eliminated most of the free H_2O adsorbed on the surface of the KBr pellet. The IR spectrum for buddingtonite or ND_4-buddingtonite show neither a substantial decrease in the FWHH nor a splitting of the NH or ND bands (cf. Figs. 3 and 4), nor was resolution of possible overlapping bands improved. A slight decrease in the FWHH for the bands was recorded, but this did not improve the resolution of the component bands for the degenerate states described above. This implies that a detailed description of the effective symmetry for the ND_4^+ and/or the NH_4^+ polyhedron is not possible from IR spectra at liquid N_2 temperatures. Therefore, within the scope of this study, this justifies assigning the most intense N–H and N–D bands to vibrational transitions on the basis of T_d symmetry as a first approximation (cf. Table 1).

The relative degree of hydrogen bonding between the NH_4^+ molecule and the surrounding oxygens in buddingtonite can be estimated from comparison with the ammonium halides, e.g. NH_4Cl, NH_4Br etc. In the ammonium halides, the N–H–X hydrogen bonds are extremely weak. The N–H frequency is typically found in the vicinity of 3300 cm^{-1}. The deformation mode ν_4, which normally can be used as a clear indicator for the formation of hydrogen bonds, is generally shifted to higher energies (Plumb and Hornig 1950). In buddingtonite, comparable energies are observed at stretching frequencies of around 3295 cm^{-1} (cf. Figs. 2–4). This represents only a very slight shift in the stretching and deformation modes to higher energies. It implies that hydrogen bonding between the NH_4^+ molecule and the surrounding oxygens, at least down to 77 K, must be relatively weak, if not non-existent.

Table 3 Results of Rietveld analysis of powder XRD data of buddingtonite and ND_4-buddingtonite

(h k l)	Buddingtonite (B2) $(NH_4)[AlSi_3O_8]$				ND_4-Buddingtonite (B7) $(ND_4)[AlSi_3O_8]$			
	d [Å]	2θ [°]	I/I_{100}(obs)	I/I_{100}(calc)	d [Å]	2θ [°]	I/I_{100}(obs)	I/I_{100}(calc)
1 1 0	6.773	13.062	16.4	15.6	6.773	13.064	18.6	18.3
0 2 0	6.528	13.555	67.4	68.2	6.523	13.567	63.8	65.0
0 0 1	6.454	13.710	12.9	13.8	6.446	13.730	12.5	12.8
1 1 −1	5.916	14.964	49.3	50.0	5.918	14.961	46.4	47.3
2 0 −1	4.333	20.483	100.0	100.0	4.339	20.457	100.0	100.0
1 1 1	3.983	22.304	37.8	39.0	3.978	22.336	44.3	42.6
1 3 0	3.814	23.303	83.1	89.2	3.812	23.322	82.1	85.0
1 3 −1	3.639	24.441	10.0	10.2	3.638	24.454	9.9	9.9
2 2 −1	3.610	24.643	3.3	4.0	3.612	24.633	3.2	3.7
1 1 −2	3.464	25.701	29.6	32.0	3.462	25.718	25.0	25.8
2 2 0	3.386	26.297	75.5	78.9	3.386	26.306	82.3	84.8
2 0 −2	3.318	26.848	52.6	52.6	3.321	26.830	43.8	44.1
0 4 0	3.264	27.303	44.0	45.3	3.262	27.325	39.3	40.1
0 0 2	3.227	27.621	89.5	93.0	3.223	27.662	85.0	84.6
1 3 1	3.015	29.602	40.3	42.9	3.013	29.632	40.7	41.1
2 2 −2	2.958	30.190	18.9	19.7	2.959	30.186	17.1	17.6
0 4 1	2.913	30.672	18.5	19.7	2.910	30.707	16.5	17.5
0 2 2	2.893	30.887	15.4	17.0	2.889	30.935	14.8	15.8
3 1 −1	2.868	31.161	8.4	8.6	2.871	31.134	9.6	10.0
1 3 −2	2.770	32.289	7.1	8.4	2.769	32.312	7.0	7.6
3 1 −2	2.655	33.736	17.2	18.2	2.658	33.701	17.2	17.3
2 4 −1	2.607	34.374	23.0	24.8	2.607	34.380	22.1	22.3
3 1 0	2.588	34.629	3.6	3.5	2.589	34.627	3.9	3.7
2 4 0	2.519	35.615	12.9	12.5	2.518	35.635	13.3	12.7
3 3 −1	2.436	36.868	9.1	9.9	2.438	36.846	9.3	9.6
2 0 −3	2.381	37.753	2.4	2.1	2.381	37.761	2.0	2.1
1 1 −3	2.318	38.825	3.9	3.4	2.316	38.863	2.7	2.7
3 1 −3	2.181	41.365	2.6	2.6	2.183	41.335	2.2	2.2
0 6 0	2.176	41.468	22.8	23.3	2.174	41.514	20.8	21.0
2 4 1	2.151	41.965	6.8	6.8	2.150	41.999	6.0	6.1
4 2 −1	2.070	43.704	6.0	6.4	2.071	43.682	7.7	7.2
4 2 −2	2.056	44.007	6.5	7.0	2.058	43.972	6.3	6.1
2 2 2	1.991	45.514	8.2	8.0	1.989	45.582	7.8	7.8
4 0 0	1.981	45.777	8.0	7.8	1.981	45.777	10.3	10.4
4 2 0	1.895	47.964	3.5	3.6	1.896	47.954	3.7	4.0
4 2 −3	1.865	48.806	5.5	5.0	1.866	48.775	5.0	4.7
1 1 3	1.858	48.978	3.8	4.0	1.856	49.055	3.6	3.6
0 6 2	1.804	50.553	8.4	9.0	1.802	50.627	7.7	8.0
2 0 −4	1.796	50.790	37.1	36.5	1.795	50.838	30.8	30.6
2 4 2	1.761	51.890	4.7	5.5	1.759	51.956	5.5	5.4
5 1 −3	1.663	55.202	4.5	4.5	1.665	55.130	4.4	4.2
4 2 −4	1.608	57.249	3.4	3.4	1.609	57.222	2.9	3.0
0 2 4	1.566	58.916	3.8	3.5	1.564	59.028	3.7	3.2
4 6 −1	1.541	59.993	4.3	4.1	1.541	59.998	4.1	3.7
2 8 0	1.509	61.398	17.4	18.1	1.508	61.452	16.7	16.5
5 3 0	1.489	62.316	2.7	2.5	1.489	62.323	3.3	3.3
5 5 −2	1.461	63.656	5.2	5.5	1.462	63.607	5.4	5.3
2 4 3	1.448	64.290	4.5	4.4	1.446	64.395	4.2	4.1
4 0 2	1.430	65.174	3.9	4.0	1.429	65.255	4.9	4.8
2 8 2	1.287	73.564	6.8	7.0	1.285	73.682	6.6	6.5

The isotopic relation for the triply degenerated states for buddingtonite and ND_4-buddingtonite, assuming T_d symmetry, is $\nu_3^D\nu_4^D/\nu_3^H\nu_4^H = 0.5647$. This value is within the usual range of agreement with the harmonic approximation value of 0.5528 (Wagner and Hornig 1950).

Rietveld refinement

Rietveld analyses were performed for all synthesis runs yielding nearly pure buddingtonite. In addition, synthesised deuterated buddingtonite, natural buddingtonite from Menlo Park, California, and two synthetic potassium feldspars were refined for comparison. All data concerning the Rietveld analysis of either phase, along with the obtained phase proportions, are given in Table 2. For all refinements, the obtained statistical parameters were within the range which indicates a good fit (cf. Table 2). Reflection positions and the relative intensities for the first 50 strongest peaks for buddingtonite synthesis B2 and one of the three ND_4-buddingtonite syntheses are given in Table 3. In Fig. 5, the corresponding observed and calculated X-ray patterns are shown. Cell dimensions for each sample,

Table 4 Cell dimensions of buddingtonite, ND_4-buddingtonite and K-feldspar

Phase	*a* (Å)	*b* (Å)	*c* (Å)	*β* (°)	Vol (Å^3)	Source
Buddingtonite B1	8.8268(7)	13.0641(9)	7.1935(5)	116.108(3)	744.87(11)	This study
Buddingtonite B2	8.8251(6)	13.0553(8)	7.1896(5)	116.142(3)	743.60(11)	This study
Buddingtonite B3	8.8262(7)	13.0574(9)	7.1882(6)	116.121(6)	743.81(12)	This study
Buddingtonite B4	8.8326(12)	13.0445(15)	7.1875(8)	116.220(6)	742.91(20)	This study
Buddingtonite B5	8.8347(8)	13.0574(10)	7.1926(6)	116.162(6)	744.72(13)	This study
Buddingtonite B6	8.8398(11)	13.0411(14)	7.1868(8)	116.285(6)	742.84(18)	This study
Deuterated Buddingtonite	8.8359(11)	13.0461(14)	7.1871(8)	116.253(6)	743.03(19)	This study
Natural Buddingtonite[a]	8.804(2)	13.040(3)	7.193(2)	116.075(24)	741.8(3)	This study
Natural Buddingtonite	8.804(3)	13.024(3)	7.183(1)	116.105(18)	739.6(3)	Kimball and Megaw (1974)
Orthoclase 1[b]	8.6050(8)	13.0154(11)	7.1851(6)	116.017(3)	723.17(14)	This study
Orthoclase 2[b]	8.6054(9)	13.0209(12)	7.1857(6)	116.032(6)	723.47(15)	This study
Natural Orthoclase	8.600	13.020	7.220	116.1	726.3	Chao et al. (1940)

[a] Natural sample from Menlo Park, California
[b] Synthesized at 500 °C, 200 MPa from a stoichiometric mixture of SiO_2, Al_2O_3 and K(OH)

Table 5 Microprobe analyses of synthetic buddingtonite

Sample analyses	B1 10	B2 9	B4 7
$(NH_4)_2O$	10.38(13)	10.42(13)	10.32(21)
SiO_2	68.51(55)	68.50(42)	68.44(45)
Al_2O_3	19.49(60)	19.57(34)	19.75(36)
Total	98.38	98.49	98.51
Atoms pfu[a]			
$^{IX}NH_4$	1.05	1.05	1.04
^{IV}Si	2.99	2.98	2.98
^{IV}Al	1.00	1.01	1.01

[a] Calculated on the basis of eight O atoms

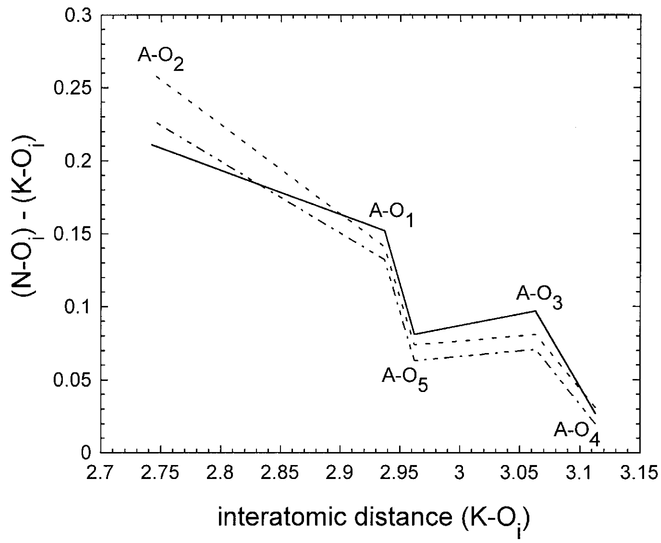

Fig. 6 Representative plot of the difference between N–O_i and K–O_i interatomic distances, i.e. A–O_i = N–O_i − K–O_i, as a function of interatomic distance K–O_i in orthoclase for three buddingtonite syntheses, i.e. B1 (*solid line*); B2 (*dash-dot line*); and B4 (*dotted line*). Buddingtonite syntheses B1–B6 and the ND_4-buddingtonite synthesis show exactly the same pattern within experimental error

refined using the Rietveld technique, are listed in Table 4.

In buddingtonite the NH_4^+ molecule replaces the K^+ cation in the orthoclase structure on the nine-fold co-ordinated A position with *m* site symmetry. Due to the larger radius of NH_4^+ in comparison to K^+, i.e. 1.69 vs. 1.52 Å, the polyhedron enclosing the NH_4^+ molecule is expanded with N–O distances ranging from 2.95 to 3.16 Å. However, these individual interatomic distances did not expand as a function of their length. Rather, the shorter the original K–O_i distance in orthoclase, the larger the expansion of the corresponding N–O_i distance in buddingtonite (cf. Fig. 6) with the interatomic N–O_2 and N–O_1 distances showing the greatest increase. The one exception to this trend is the N–O_5 distance, which exhibits a relatively smaller increase in length (cf. Fig. 6).

In general, the A-site polyhedron in buddingtonite is expanded in such a way that it becomes more regular in comparison to the A-site polyhedron in orthoclase. To compensate for this expansion, the Al, Si framework responds via rotation of the rigid Al, Si tetrahedra. This is obvious from the changes in the $T_{1,2}$–O_i–$T_{1,2}$ angles, which are correlated to the changes in the interatomic distances. Because of this expansion in the interatomic distances, the unit-cell parameters for buddingtonite are larger when compared to natural and synthesised potassium feldspars (cf. Table 4). This is especially seen with respect to the lattice parameter *a* and the monoclinic angle *β* which are the most influenced by the substitution of NH_4^+ for K^+. In contrast, within experimental error, the magnitude of the *b* and *c* lattice parameters remains nearly unchanged.

The strong influence on the magnitude of *a* and *β* from the substitution of NH_4^+ for K^+ is also evident from investigations of natural buddingtonites. For example, a sample of buddingtonite from Sulphur Bank, Lake County, California (Kimball and Megaw 1974), which contains a 5 mol% orthoclase component, has markedly smaller values for *a* and *β* compared to pure end-member synthetic buddingtonite (cf. Table 4). This effect is also seen for a sample of natural buddingtonite from Menlo Park, California, investigated in this study (cf. Table 4). The obtained cell dimensions for this sample are in good agreement with those given by Kimball and Megaw (1974) for the buddingtonite from Sulphur Bank and suggest the presence of a minor orthoclase component similar to that seen in the Sulphur Bank sample.

Lattice parameters obtained for a series of synthetic buddingtonites (B1 to B6) were found to be extremely variable with respect to the lattice constants *a* and *b* and also the monoclinic angle β, lying outside experimental error (cf. Table 4). Yet all samples from B1 to B6 were synthesised under the same pressure-temperature conditions with one exception: for B1 the synthesis temperature was lowered from 500 to 400 °C. Cell dimensions obtained for the synthetic deuterated buddingtonite also fall within this range (cf. Table 4). These variations in the cell parameters are unlikely to be due to differences in chemical composition since they were all synthesised under relatively the same conditions from the same stoichiometric SiO_2–Al_2O_3 oxide mix and 25% NH_3 solution. Microprobe analysis of samples B2 and B4 indicated, within analytical error, no evidence for variations in the chemical composition. However, since the error in the electron microprobe measurement of nitrogen is relatively large, some uncertainty does exist as to whether or not incorporation of H_3O^+ instead of NH_4^+ or zeolitic water could play a role in this variability. The incorporation of either H_3O^+ or zeolitic water could distort the unit-cell lattice in buddingtonite as well as be responsible for the variability in the unit-cell parameters seen in Fig. 6, since each buddingtonite synthesis could take in variable amounts of either type. However, careful IR measurements of samples B2 and B4, which were both at different extremes in the range of unit-cell variability, indicated that neither sample contained H_3O^+ or zeolitic water.

It is also quite possible that these trends could be caused by structural variations such as the Al, Si distribution. This is certainly the cause of deviations in unit-cell parameters for natural and synthetic orthoclases (Kroll and Ribbe 1987). However, Al, Si ordering in the unit-cell lattice for orthoclase leads only to variations in the *b* and *c* directions. In contrast, the lattice parameter *a* and the monoclinic angle β should remain nearly unaffected. In the case of the buddingtonites synthesised for this study, we observe variations in the magnitude of the *b* lattice constant outside experimental error which certainly could be caused by Al, Si ordering on the T_1 and T_2 sites. However, the observed variability in the *a* lattice parameter is highly unlikely to be caused by Al, Si ordering. This is because along the *a* direction in the lattice unit cell, the number of T_1 and T_2 tetrahedra are the same (Kroll and Ribbe 1987). In this context, while the substitution of NH_4^+ for K^+ and the corresponding expansion of the A site could play an important role with respect to the variability of the *a* and β unit-cell parameters, most likely, both expansion of the A site and Al, Si disorder have some influence on the variability of the *a* and *b* lattice parameters and the β monoclinic angle.

Acknowledgements We thank Ursula Glenz and Helga Kemnitz for assistance with the SEM and Inka Bauer for preparing the KBr discs for IR. B. Pöter thanks Matthias Gottschalk for introduction to the Rietveld technique as well as many useful discussions. B. Pöter also thanks Dieter Rhede and Oona Applet for assistance with the microprobe. M. Andrut thanks Björn Winkler for useful discussions. This project was supported by a German Science Foundation grant (He 2015-5) to Wilhelm Heinrich.

References

Barker DS (1964) Ammonium in alkali feldspars. Am Mineral 49: 851–858

Bastoul AM, Pironon J, Mosbah M, Dubois M, Cuney M (1993) In situ analysis of nitrogen in minerals. Eur J Miner 5: 233–243

Beran A, Armstrong J, Rossman GR (1992) Infrared and electron microprobe analysis of ammonium ions in hyalophane feldspar. Eur J Miner 4: 847–850

Chao SH, Hargreaves A, Taylor WH (1940) The structure of orthoclase. Mineral Mag 25: 498–512

Dollase WA (1986) Correction of intensities for preferred orientations of the March model. J Appl Crystallogr 19: 267–272

Erd RC, White DE, Fahey JJ, Lee DE (1964) Buddingtonite, an ammonium feldspar with zeolitic water. Am Mineral 49: 831–850

Griffiths PR, de Haseth JA (1986) Fourier transform infrared spectroscopy. In: Chemical analysis, vol 83. Wiley, New York

Gulbrandsen RA (1974) Buddingtonite, ammonium feldspar, in the Phosphoria Formation, southeastern Idaho. J Res US Geol Surv 2(6): 693–697

Hall A (1988a) Crustal contamination of minette magmas: evidence from their ammonium contents. N Jb Miner Mnt 1988: 137–143

Hall A (1988b) The distribution of ammonium in granites from southwest England. J Geol Soc London 145: 37–41

Hall A (1993) The influence of secondary alteration on the ammonium content of granites exemplified by the Rosses complex of Donegal. Mineral Mag 57: 591–598

Hall A, Stamatakis MG, Walsh JN (1994) Ammonium enrichment associated with diagenetic alteration in Tertiary pyroclastic rocks from Greece. Chem Geol 118: 173–183

Hall A, Pereira MD, Bea F (1996) The abundance of ammonium in the granites of central Spain and the behaviour of the ammonium ion during anatexis and fractional crystallisation. Miner Petrol 56: 105–123

Hallam M, Eugster HP (1976) Ammonium silicate stability relations. Contrib Miner Petrol 57: 227–244

Herzberg (1955) Infra-red and Raman spectra of polyatomic molecules. Van Nostrand, New York

Higashi S (1982) Tobelite, a new ammonium dioctahedral mica. Miner J 11(3): 138–146

Honma H, Itihara Y (1981) Distribution of ammonium in the minerals of metamorphic and granitic rocks. Geochim Cosmochim Acta 45: 983–988

Hori H, Nagashima K, Yamada M, Miyawaki R, Marubishi T (1986) Ammonioleucite, a new mineral from Tatarazawa, Fujioka, Japan. Am Mineral 71: 1022–1027

Johannes W (1973) Eine vereinfachte Piston-Zylinder-Apparatur höher Genauigkeit. N Jb Miner 1973: 337–351

Kimball MR, Megaw HD (1974) Interim report on the crystal structure of buddingtonite. NATO Advanced Study Institute, University of Manchester, Manchester, England: 81–86

Krohn MD, Altaner SP (1987) Near-infrared detection of ammonium minerals. Geophysics 52: 924–930

Krohn MD, Kendall C, Evans JR, Fries TL (1993) Relations of ammonium minerals at several hydrothermal systems in the Western US. J Volcan Geotherm Res 56(4): 401–413

Kroll H, Ribbe PH (1987) Determining (Al, Si) distribution and strain in alkali feldspars using lattice parameters and diffraction-peak positions; a review. Am Mineral 72: 491–506

Landolt-Börnstein (1951) Physikalisch-chemische Tabellen, vol 2

Laricheva OO, Akhmanova MV, Bychkov AM (1993) Low-temperature hydrothermal synthesis of buddingtonite. Geochem Int 30: 126–132

Laricheva OO, Akhmanova MV, Bagmut NN, Kalinchenko AM, Kuznetsova TP, Bychkov AM (1996) NH_4^+-bearing sanidines: synthesis and estimation by X-ray diffraction, infrared spectroscopy, ESR, and PMR. Geochem Int 33: 74–80

Larson AC, von Dreele RB (1987) Generalized structure analysis system. Los Alamos National Laboratory Rep LAUR 86-748

Loughnan FC, Roberts FI, Lindner AW (1983) Buddingtonite (NH_4-feldspar) in the Condor oilshale deposit, Queensland, Australia. Mineral Mag 47: 327–334

March A (1932) Mathematische Theorie der Regelung nach der Korngestalt. Z Kristallogr 81: 285–297

Marfil R, Hall A, Garcia GS, Stamatakis MG (1998) Petrology and geochemistry of diagenetically altered tuffaceous rocks from the Middle Triassic of central Spain. J Sed Res (A): Sed Petrol Proc 68: 391–403

Mertz L (1965) Transformation in optics. Wiley, New York

Nakamoto K (1986) Infrared and Raman spectra of inorganic and co-ordination compounds. Wiley, New York

Plumb RC, Hornig DF (1950) Infrared spectrum, X-ray diffraction pattern, and structure of ammonium fluoride. J Chem Phys 23: 947–953

Ramseyer K, Diamond LW, Boles JR (1993) Authigenic K-NH_4-feldspar in sandstones: a fingerprint of the diagenesis of organic matter. J Sed Petrol 63: 1092–1099

Solomon GC, Rossman GR (1988) NH_4^+ in pegmatitic feldspars from the southern Black Hills, South Dakota. Am Mineral 73: 818–821

Voncken JHL, Konings RJM, Jansen JBH, Woensdregt CF (1988) Hydrothermally grown buddingtonite, an anhydrous ammonium feldspar ($NH_4AlSi_3O_8$). Phys Chem Miner 15: 323–328

Voncken JHL, van Roemund HLM, van der Eerden AMJ, Jansen JBH, Erd RC (1993) Holotype buddingtonite: an ammonium feldspar without zeolitic H_2O. Am Mineral 78: 204–209

Wagner EL, Hornig DF (1950) The vibrational spectra of molecules and complex ions in crystals. III. Ammonium chloride and deutero-ammonium chloride. J Chem Phys 18: 296–304